Philosophical Magazine,
Vol. 86, No. 27, 21 September 2006, 4195–4212

Taylor & Francis
Taylor & Francis Group

The elastic field of general-shape 3-D cracks

N. M. GHONIEM*† and J. HUANG‡

†Mechanical and Aerospace Engineering Department, University of California, Los Angeles, CA 90095-1597, USA
‡The Titan Corporation, 3394 Carmel Mountain Road, San Diego, CA 92121-1002, USA

(*Received 28 June 2005; in final form 8 September 2005*)

We extend here the Bilby-Eshelby approach of 2-D crack representation with dislocation pileups to treat 3-dimensional cracks of general geometry. Cracks of any specified external bounding 3-D contour under general loading conditions are represented by sets of parametric Somigliana loops that satisfy total (interaction, self, and external) force equilibrium. Loop positions are solved by using a time integration scheme till equilibrium is achieved. The local Burgers vector is suitably adjusted to be proportional to the local applied surface traction on the crack. The developed method is computationally advantageous, since accurate crack stress fields are obtained with very few concentric parametric loops that adjust to the external crack shape and the local force conditions. The method is tested against known elasticity solutions for 3-D cracks and found to be convergent with an increase in the number of pileup dislocation loops. The method is applied to the determination of the stress field around a 3-D Griffith crack under general loading and a grain boundary crack before and after branching.

1. Introduction

The connection between fracture and dislocations has been established during the past few decades [1–5]. Based on the work of Eshelby in the early 1950's, and later by Bibly, Cottrell and Swinden(BCS) [6], Bibly and Eshelby [3], and many others, a continuous distribution of dislocations was utilized to determine the elastic field of two-dimensional cracks (i.e. under plane stress of plane strain conditions). Since the dislocation line in the most general sense (Somigliana dislocation) represents the boundary across which a displacement jump takes place, a collection of such boundaries may be pieced together to match the Crack Opening Displacement (COD) under specified load conditions. When the displacement jump is variable along the dislocation line, we have the Somigliana dislocation, while if it is a fixed vector (the Burgers vector), the Volterra dislocation is obtained. Both types are possible in continuous solids. However, in a crystal lattice, the displacement jump is fixed and constrained by the crystal structure. We will hence differentiate dislocations in crystalline materials as crystal dislocations, which are associated with plastic deformation, while Somigliana or Volterra dislocations used to represent cracks will be termed crack dislocations. In this way, a crack in an elastic–plastic

*Corresponding author. Email: ghoniem@ucla.edu

Philosophical Magazine
ISSN 1478–6435 print/ISSN 1478–6443 online © 2006 Taylor & Francis
http://www.tandf.co.uk/journals
DOI: 10.1080/14786430500343843

material can be viewed as a distribution of Somigliana or Volterra dislocations on the crack plane, associated with another distribution of crystal dislocations within the plastic zone of the crack tip.

The similarity between cracks and dislocation pileups was first recognized by Eshelby, Frank and Nabarro [1]. Using classical orthogonal polynomials, they determined the equilibrium of a discrete dislocation pileup under external loading. For simple loading conditions, the dislocation distribution function can be analytically obtained. The stress field generated by the dislocation pileup was shown to be identical to that of a crack with freely slipping surfaces. An equivalent method, in which a continuous distribution function is assumed, was first suggested by Leibfried [7]. Instead of dealing with discrete dislocations, the slip plane is assumed to contain a smeared-out sheet of infinitesimal dislocations, with a distributed displacement jump of $bf(x)dx$ between x and $x+dx$, where x is the position on the crack surface in 2-D. Thus the problem is converted to finding an unknown distribution function, $f(x)$, by solving the following singular integral equation:

$$P\int_{-\infty}^{\infty}\frac{f(x')dx'}{x'-x}=F(x) \tag{1}$$

where P and $F(x)$ are determined by the boundary conditions and applied load. Friedel [8, 2] first described a crack with a normal displacement discontinuity by a continuous distribution of freely climbing dislocations. Later, a detailed discussion of crack dislocations was given by Bibly and Eshelby [3], where dislocations were considered as discontinuities occurring naturally across un-welded cuts when a body is stressed, while in a crystal dislocation, the cuts are subsequently rewelded.

When the thickness of the crack is finite, it can no longer be represented by 2-D infinitely-long and straight dislocations. The stress field of a 3-D crack can be obtained if one assumes that the surface is filled with a distribution function of infinitesimal dislocation loops. Since the stress field of an infinitesimal loop can be analytically obtained [9, 10] for an isotropic elastic material, the equilibrium equation for the crack surface results in a hyper-singular integral equation of the form

$$\int_S\frac{f(x',y')dS}{r^3}=\sigma^0(x,y) \tag{2}$$

where, $r=\sqrt{(x-x')^2+(y-y')^2}$, S is crack surface, and $\sigma^0(x,y)$ is a known function determined by the load and boundary conditions. Once the distribution function is obtained, the stress field of the crack is completely determined [3].

For 2D applications, the distribution method provides an easy way to solve problems involving the interaction of cracks and dislocations. For example, since the shielding stress of screw crystal dislocations situated ahead of a mode-III crack tip can be easily obtained from image screw dislocations, full elastic–plastic analysis of mode-III cracks has been developed and used by many researchers. In all other cases, however, determination of image forces due to the free surface of the crack is more involved. Lardner [4] and Weertman [5] document the method of solving crack problems in elastic–plastic solids with the aid of 2-D continuous dislocation distributions. Instead of the analytical solutions to equation (1), Hills *et al.* [11] developed a numerical scheme for the distribution function for 2-D and 3-D cracks, and showed that the technique is more efficient than the finite element procedure.

The objective of the present work is to extend the 2-D discrete representation method to treat elasticity problems for general 3-D cracks and crack-dislocation applications. Parametrization of crack surfaces with discrete dislocation loops will enable extensions of the Parametric Dislocation Dynamics (PDD) method [12–15] to fracture problems. Although the original thrust of the PDD method has been in simulations of plasticity, the present extension would make it possible in the future to model complex fracture problems involving both dislocation and crack ensembles. The method of representing 3-D cracks with dislocation pileups is given in section 2, where we describe the current theoretical and computational approach. Numerical results for the stress field of standard 3-D cracks are given in section 3, and compared to known solutions to ascertain the numerical validity of the present method. An illustration of the utility of the method for complex-shape cracks is given in section 4, where we determine the elastic field around a Griffith crack under complex loading, and a branched 3-D grain boundary crack. This is followed by discussion and conclusions in section 5.

2. Computational method

The stress state around a crack in an elastic body subjected to general external loading is identical to the superposition of the following two contributions [16]:

- The stress generated in a crack-free body, subject to the external loading alone.
- The stress generated by the crack in the same body subject to a set of internal tractions alone. This set represents counter-forces to those acting on welded crack surfaces determined from the previous step.

The procedure is illustrated in figure 1, and is as follows. Firstly, we determine the elastic field of the crack-free solid (i.e. the crack surfaces are welded) under the applied load $\mathbf{T}_1$ & $\mathbf{T}_2$. The stress distribution $\boldsymbol{\sigma}_1$ is thus obtained, and the force vectors along the crack surface $\mathbf{T}_x$ & $\mathbf{T}_y$ determined. The second step is to apply the counter-force system $-\mathbf{T}_x$ & $-\mathbf{T}_y$ on the crack surface and solve for the stress distribution $\boldsymbol{\sigma}_2$. The final stress distribution by the superposition of $\boldsymbol{\sigma}_1$ and $\boldsymbol{\sigma}_2$.

Friedel [2], and Bibly and Eshelby [3] proposed a dislocation method that is equivalent to the previous procedure proposed by Bueckner [16]. Suppose that the crack is filled with the same material layer by layer and then welded together, as shown in figure 2. Under the applied load, the stress field can be obtained as $\boldsymbol{\sigma}^A$. On the other hand, each inserted material strip will generate a displacement jump, and utilizing Green's functions, the stress field due to the inserted strip is obtained. In this way, each strip can be viewed as a dislocation loop. In 2-D crack applications, the crack is assumed to be infinitely long in one direction. Thus, the material strip must also be infinite in one direction, and the corresponding dislocation loop can be assumed to be a dislocation dipole with two infinitely long and straight dislocations of opposite line directions. In this case, the stress field can be obtained analytically, and the total stress generated by these dislocation loops can be written as

$$\boldsymbol{\sigma}^D(x) = \mathbf{A} \int \frac{D(x')dx'}{x - x'} \tag{3}$$

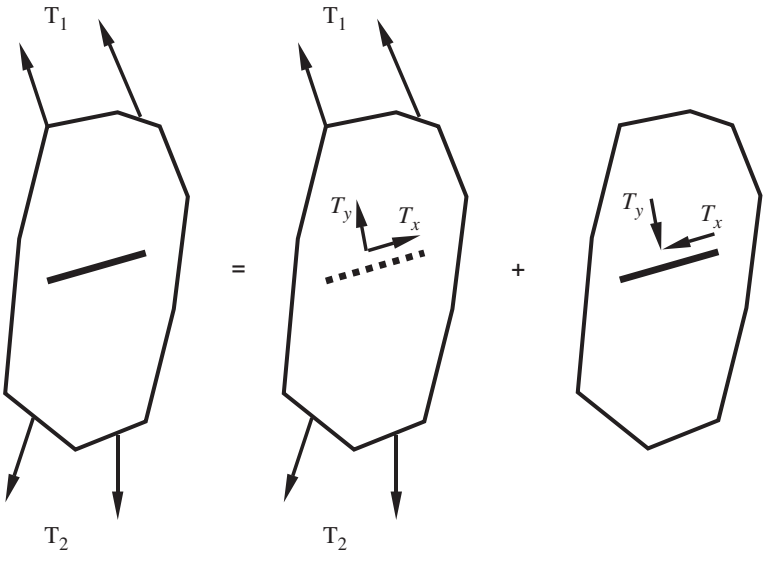

Figure 1. Illustration of the superposition method for the solution of the general crack problem [16].

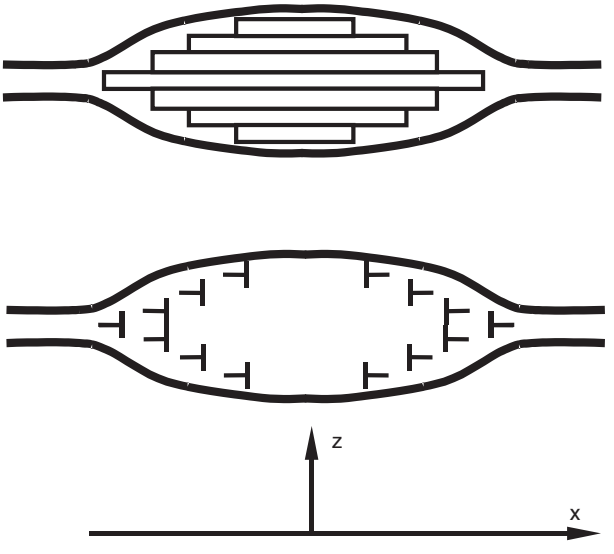

Figure 2. Eshelby's interpretation of crack dislocations by material insertion.

where, **A** is a constant second rank tensor related to the applied loading and elastic constants. $D(x')$ is a scalar distribution function representing the dislocation density between x' and $x'+dx'$. Thus, the total stress field $\boldsymbol{\sigma}$ in the solid is

$$\boldsymbol{\sigma} = \boldsymbol{\sigma}^A + \boldsymbol{\sigma}^D. \tag{4}$$

This solution technique is identical to the Bueckner procedure [16]. Thus, the main problem is to obtain the distribution function $D(x')$ by solving a singular integral equation, as described below. On the crack surface, the free traction boundary condition gives for the total traction vector

$$\begin{aligned} \mathbf{T}^{\text{tot}} &= \mathbf{T}^A + \mathbf{T}^D = 0 \\ (\boldsymbol{\sigma}^A(x) + \boldsymbol{\sigma}^D(x)) \cdot \mathbf{n} &= 0 \\ \boldsymbol{\sigma}^A(x) + \mathbf{A} \int \frac{D(x')dx'}{x - x'} &= 0. \end{aligned} \tag{5}$$

For finite size cracks, Bibly and Eshelby [3] assumed that the crack surface is filled with infinitesimal dislocation loops. By solving similar singular integral equations, one can obtain the total field of 3-D cracks. However, and in practice, the numerical implementation of this method is cumbersome and requires intensive calculations for geometrically complex cracks. We present here an alternative simpler method for determination of the stress field around general-shape 3-D cracks under arbitrary loading conditions.

The current strategy is that we use a discrete representation of the displacement discontinuities across the crack surfaces instead of continuous distribution functions. We also assume that the crack surface is filled with pileups of dislocation loops (representing material strips) in mechanical equilibrium, much the same way as used for the solution of 2-D problems. The position and shape of each dislocation loop are determined by configurational force balance principles. Thus, the key problem is to find the configuration of each dislocation loop and its shape, consistent with the external loading and the constraint of the outside shape of the crack. Note that due to the fact that we have true 3-D conditions, the crack dislocation is the general Somigliana type. Configurational force equilibrium at every point of a dislocation loop is given by

$$\mathbf{F}_{\text{tot}} = (\boldsymbol{\sigma}^A + \boldsymbol{\sigma}^I + \boldsymbol{\sigma}^S) \cdot \mathbf{b} \times \mathbf{s} = 0 \tag{6}$$

where, $\boldsymbol{\sigma}^A$, $\boldsymbol{\sigma}^I$ and $\boldsymbol{\sigma}^S$ are the local stresses at the point of interest generated by the applied loads, interaction forces from other loops, and the self-stress, respectively. $\mathbf{F}_{\text{tot}}$ is the total force, $\mathbf{b}$ is a local Burgers vector and $\mathbf{s}$ is the tangent vector to the loop at the current point. Note that equation (6) is a discrete form of equation (5) and that both represent the equilibrium equation for the crack surface. The dislocation stress, $\boldsymbol{\sigma}^D(x)$, given by the integral term in equation (5), is equivalently computed by discretely summing the interaction stress, $\boldsymbol{\sigma}^I$, and the dislocation self stress (because of curvature) $\boldsymbol{\sigma}^S$. Reference [4] gives a more detailed discussion of the correspondence between the discrete and continuous representations of cracks.

Recall that the governing equations of motion of dislocation loop are obtained from the second law of thermodynamics and expressed as [14]

$$\oint_{\Gamma} (\mathbf{F}_{\text{tot}} - B\mathbf{V}) \cdot \delta\mathbf{r} |ds| = 0 \tag{7}$$

where $\mathbf{V}$ is a local velocity vector, B is the resistivity to dislocation motion (inverse mobility), and ds is an infinitesimal arc length on the loop. The final equilibrium state of equation (7) is reached when the total force is zero at every point on the contour Γ. Thus this equilibrium configuration is the same as required by equation (6).

The Parametric Dislocation Dynamics (PDD) method [17] has been developed to solve the equations of motion of curved dislocations (derived from equation 7), and will be employed here to solve the equilibrium conditions of a 3-D crack (equation 6). Note that Burgers vector of each dislocation loop in a crack dislocation pileup needs to be chosen carefully. In the present 3D simulation, we choose the Burgers vector to be proportional to the traction vector at the crack surface

$$\mathbf{b} = \alpha \mathbf{t} = \alpha \boldsymbol{\sigma} \cdot \mathbf{n} \tag{8}$$

where $\mathbf{n}$ is the unit normal vector to the crack surface, $\mathbf{t}$ the traction (stress) vector, and α is a control constant. If the applied load is not uniform, the local Burgers vector will be variable along the loop, and hence the crack dislocation is of the general Somigliana-type. To achieve high numerical precision the constant α should be small since more dislocation loops can be fitted within the crack surface. The selection of the local Burgers vector in accordance with equation (8) is motivated by considering the limiting behaviour of the displacement vector as a point force is applied to the crack surface, when one approaches the point of application along the point force direction. The Green's tensor functions, G_{ij} give the displacement in direction (i) for a point force in direction (j). If we consider the isotropic Green's functions and take the limit of field point approaching the source point (on the crack surface) along the force direction, one can easily show that the off-diagonal terms are zero, and that the displacement vector is aligned along the force vector, with a magnitude of $(4\pi\mu R)^{-1}$, where R is the distance between field and source points. Equation (8) is a statement of this analysis, where the displacement vector at the crack surface is aligned with the traction vector on the crack surface.

The current computational strategy is summarized in the following steps:

(1) An initial distribution of dislocation loops whose shape conforms with the outer crack shape is selected. The outermost loop has the exact contour of crack surface, and is fixed during the simulation. As a result of the applied stress, mutual and self interactions, each dislocation loop shape and size adjusts in order to reach total equilibrium.
(2) If the repulsive force from all loops on the innermost loop is small, the loop will expand until it reaches a new equilibrium configuration. A fresh loop is then generated at the centre with local Burgers vector determined by equation (8). Hence the total number of crack dislocations is increased by one.
(3) If the repulsive force on the innermost loop is large forcing it to fall below a critical stable size, it will collapse under its own self-forces. The loop is then taken out, and the number of crack dislocations is decreased by one.
(4) Iteration of the dynamic loop addition–subtraction process continues until a final equilibrium distribution is achieved.
(5) Utilizing the fast sum method [18] for each curved loop segment, the stress field of the entire crack is finally obtained.

3. Numerical results and method validation

The method developed here allows for the efficient computation of the stress field around 3-D cracks of general geometry. It can be applied to finite geometry with

multiple interacting cracks, including the influence of free surfaces or interfaces. Before we demonstrate the utility of the approach in analyzing a branched grain boundary crack, we will first ascertain the numerical accuracy of the method in this section, and extend the loading conditions for some of the most widely analyzed cracks.

3.1. *The penny-shape crack*

The stress field in an infinite solid containing a penny-shape crack provides a benchmark for fracture mechanics studies, and has thus been developed for various loading conditions and geometries. Sack [19] and Sneddon [20] first solved the problem of a penny-shape crack with an internal pressure in an infinite solid, while Collins [21] later investigated the stress distribution of a penny-shape crack in a thick plate. Kassir and Sih [22] studied an elliptical crack under arbitrary external loading, and obtained results for the stress intensity factors under shear loading. Here, we present numerical results for the current method applied to a penny-shape crack under tension or shear loading, and then compare the results to analytical solutions.

Mode-II. Consider a penny-shape crack in an isotropic crystal with diameter of $2000a$, where a is a specified length scale related to the magnitude of the Burgers vector, as shown in figure 3a. The crack is under pure shear loading along the x-axis. The local coordinate system is constructed at the centre of the crack. An initial distribution of circular dislocation loops is inserted inside the crack, with a minimum of 3 loops, including the outermost static loop that defines the crack contour. The applied load generates a uniform shear stress field in the absence of the crack. Thus, according to equation (8), the Burgers vector can be chosen as $\mathbf{b} = b\mathbf{i}$, where b is a constant scalar, and can be adjusted to achieve a specified level of error, and $\mathbf{i}$ is a unit vector along the x-axis. Since the Burgers vector is uniform and lies on the glide plane, this type of crack dislocation is a traditional Volterra dislocation.

Figure 3b illustrates the final equilibrium distribution of crack dislocations under the applied shear load $\tau/\mu = 0.004$, where μ is the shear modulus. The length of the Burgers vector is chosen as $b = 0.4a$, and Poisson's ratio $\nu = 0.31$. As shown in the

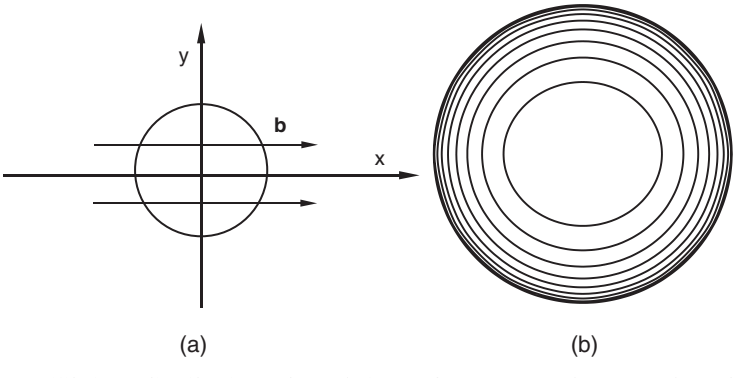

Figure 3. Equilibrium distribution of crack loops for a penny-shape crack under mode-II ($\sigma_{zz}/\mu = 0.004$). (a) The local coordinate system, (b) Equilibrium distribution.

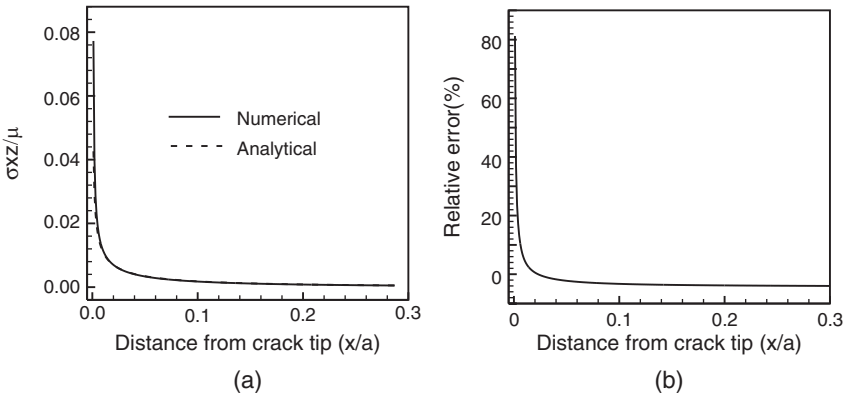

Figure 4. Comparison of the calculated stress component σ_{zz}/μ along the y-direction with the analytical solutions of Kassir and Sih [22] (a) σ_{zz}/μ. (b) The relative error.

figure, a total of 9 dislocation loops are fitted within the crack surface in a pileup that is stabilized by the applied stress. Since the energy of a screw segment of unit length is lower than a corresponding edge segment, a curved screw component tends to be stiffer than that of the edge. Thus, initially circular loops tend to stretch along the Burgers vector in an oval configuration. As the outer contour of the crack is circular, a slight ovality develops in the innermost loops. The minimum distance between the two outermost loops is around $10b$, and 16 quadrature points are for Gaussian integration [18].

The distribution of the shear stress σ_{xx}/μ along the y-direction is shown in figure 4a, while the relative error is displayed in figure 4b. The comparison is with the analytical solutions of Kassir and Sih [22]. Beyond a short distance of $\approx 10a$ from the crack tip, the stress decays rapidly and tends to vary slowly at longer distances from the tip. The stress field is no longer proportional to $r^{-1/2}$ as in the case of two dimensional cracks. When the distance is less than $5a$, the relative error is larger than 10%. As shown in reference [18], the relative error in the stress generated by a dislocation loop tends to be higher when the field point approaches the dislocation loop. To reduce the near tip error, shorter curved segments and/or a larger number of Gaussian quadrature points are needed. In the present simulations, we use 16 quadrature points only, resulting in a relative error of less than 5% at distances longer than $10a$ from the tip of the crack.

Mode-I. The surfaces of a penny-shape crack subject to pure tensile loading normal to the unloaded crack plane displace along the tensile axis. If the displacement profile is to be recovered by the insertion of dislocations, one would expect that such dislocation loops must be prismatic, with their Burgers vectors along the tensile axis, and that they would also climb along their prismatic surfaces. We simulate here a penny-shape crack loaded in tension with an initial distribution of prismatic edge Volterra dislocation loops of constant and uniform Burgers vectors selected according to equation (8) as $\mathbf{b} = b\mathbf{k}$, where $\mathbf{k}$ is a unit vector along the tensile direction. Sneddon [20] has obtained analytical solutions to the same problem enabling us to determine the numerical features and precision of the present method.

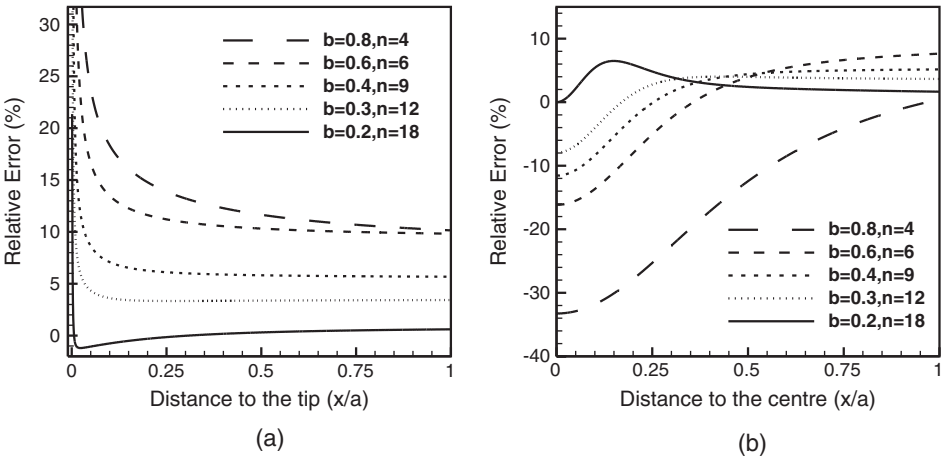

Figure 5. Comparison of the relative error in σ_{zz} for the penny-shape crack under the external loading $\sigma_{zz}/\mu = 0.004$. (a) along the radial direction, (b) along the tensile direction.

Table 1. The relative percent error in σ_{zz} along the radial direction of a penny-shape crack under mode-I loading. The number of concentric loops is shown in the first row, and the value in brackets is the length of the Burgers vector in each case. The first column is for the distance from the crack tip. All distances are in units of a; an arbitrary length scale.

d:n	4 (0.8)	6 (0.6)	9 (0.4)	12 (0.3)	18 (0.2)
2	166.39	109.97	57.16	32.60	7.65
5	91.00	58.16	28.80	15.33	0.64
10	57.32	36.62	18.21	9.42	−0.87
20	37.42	24.65	12.55	6.38	−1.20
50	23.82	16.64	8.64	4.34	−1.06
100	18.35	13.48	7.09	3.61	−0.76

Figure 5 and table 1 present a comprehensive assessment of the method's accuracy, and point out to the means of controlling the numerical precision in the stress field. The information would naturally be useful in applications where no such analytical results exist. The relative error in σ_{zz} along the tensile z-direction obtained from the present method is compared with the analytical results of Sneddon [20]. It is shown that, when the length of the Burgers vector is increased, mutual repulsive forces between concentric dislocation loops are large, and the final stable number of dislocation loops is small. Large field errors are associated with a small number of loops. For example, when $b = 0.8a$, only 4 concentric loops are sufficient to represent the crack, albeit at the expense of a high relative error (e.g. 91.00% at a distance of $5a$ from the tip). When b decreases to 0.2a, 18 dislocation loops equilibrate inside the crack, and the same error decreases to 7.65%. The stress field is convergent to any desired accuracy, if a sufficient number of dislocation loops is used. However, the computational burden increases significantly for larger populations of dislocation loops, and efficient computational and theoretical methods are thus required, as outlined in references [17, 23]. The relative error of σ_{zz} along the z-axis is shown in

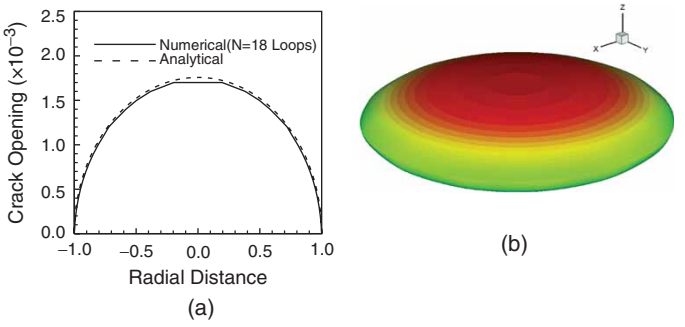

Figure 6. Comparison of the numerical results for the Crack Opening Displacement (COD) with analytical solutions [20] for $n = 18$. (a) COD distribution along the crack diameter. (b) 3-D crack shape.

figure 5b, where it is clear that the stress at the crack centre is convergent in a controllable manner and approaches the applied stress as b decreases.

The displacement vector on the crack surface is continuous in regions in-between dislocation loops, and has a discontinuity of exactly b across any loop boundary. However, if the number of loops is sufficiently large, the 3-dimensional shape of the crack opening displacement (COD) and hence the crack shape can be reconstructed. The displacement vector field distributed inside the crack surface (i.e. the COD) vanishes on the outer crack boundary, and is used as a reference for the COD. Figure 6 shows the COD as a function of the radial distance from the crack centre. Numerical results are compared with analytical solutions [20]. When $b = 0.2$ ($n = 18$), the maximum error in the COD (at the centre) is 3.3%. This error can be made arbitrarily small with an increase in the number of loops.

3.2. *The 2-D Griffith crack*

The classical 2-D Griffith crack under simple loading has been extensively modelled with continuous and distributed dislocations, and has been used as a benchmark in fracture mechanics [4, 5]. Here, we represent the same Griffith crack with 3-D discrete dislocation distributions, and compare the results to well-known analytical solutions. Consider a finite Griffith crack of length $4000a$ in y-direction, and of width $400a$ in the x-direction. The crack surface normal is chosen along the z-direction, as illustrated in figure 7. Since the crack has a large aspect ratio (the ratio of width to length is 10), the stress field at the crack centre can be approximated by 2-D solutions. Since the two ends of the crack surface are open, we will not use closed loops as in the previous case of a penny-shape crack, but will rather introduce dislocation dipoles as the basic elements. The simulation technique here starts with two dislocations of the same Burgers vector but of opposite line direction. We allow the two dislocations in this dipole to move freely, satisfying force equilibrium. An external load keeps such pairs from attraction and annihilation. However, for every applied load, there is a critical distance between the dislocations, below which the pair is unstable and annihilates. When the separation distance between the dipoles is sufficiently large, a new dipole is added to the equilibrating set of dislocations, just as we did in the penny-shape crack.

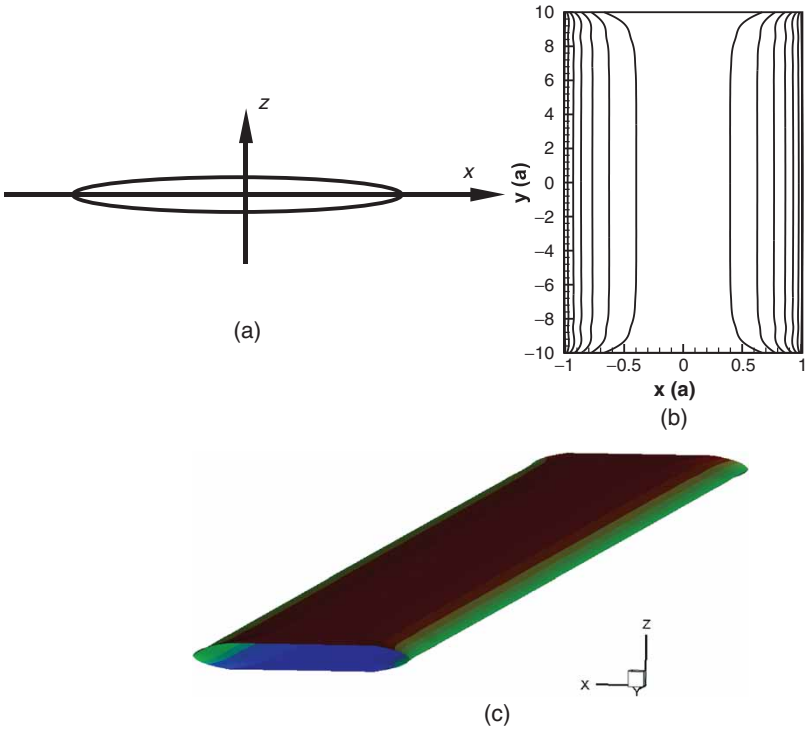

Figure 7. Distribution of crack dislocations for a Griffith crack under mode-I loading with applied tension $\sigma_{zz}/\mu = 0.004$ along the z-direction. (a) Coordinate system (b) Distribution f crack dislocations with a Burgers vector of 0.15a. (c) three-dimensional crack shape.

The Griffith crack is subjected to an applied tensile load of $\sigma_{zz}/\mu = 0.004$ along the z-direction, and the system of equilibrium equations is solved for the inserted dipoles, as outlined earlier. The distribution of crack dislocations is shown in figure 7b. It is seen here that in the middle section of the crack ($-500a \leq y \leq 500a$), dislocations are perfectly straight. Thus, the stress field in this section can be approximated by 2-D plane elasticity. The relative error of stress component σ_{zz} at the crack centre along the x-direction from the crack tip is shown in figure 8 and table 2. The number of crack dislocations is inversely proportional to the length of selected Burgers vector, as can be observed in both the table and figure. As we found in the penny-shape crack solution, when b is decreased, the solution converges to the analytical results.

4. Applications

4.1. *Complex loading of a Griffith crack*

When a Griffith crack is loaded by a general stress tensor, a mixed mode of deformation occurs. In this case, crack dislocations must perform combined glide and climb motion to reach their equilibrium state. Moreover, if the stress field

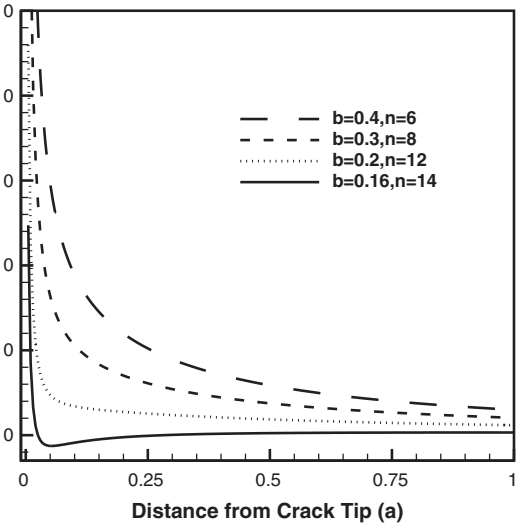

Figure 8. Comparison of the relative error in σ_{zz}; the same conditions as in figure 7.

Table 2. The relative percent error of σ_{zz} for the Griffith crack under mode-I loading. The number of dislocations is shown in the first row, and the value in brackets is the length of the Burgers vector in each case. The first column is for the distance from the crack tip. All distances are in units of *a;* an arbitrary length scale.

d:n	6(0.4)	8(0.3)	12(0.2)	14(0.16)
2	93.73	57.15	22.75	8.44
5	48.15	27.30	8.51	−0.05
10	29.64	16.38	4.73	−1.26
20	18.86	10.58	3.40	−0.88
50	10.22	6.12	2.55	−0.07
100	5.87	3.75	1.86	−0.24

is nonuniform over the crack surface, the Burgers vector on each dislocation is no longer constant, but will vary depending on the local value of the stress field, and hence the representative dislocation is of the general Somigliana type. Consider mixed mode I & II loading of the same Griffith crack presented in the previous section. We take a representative loading state with tensile component of $\sigma_{zz}/\mu = 0.004$, and a shear component $\sigma_{zz}/\mu = 0.002$. The stress tensor on crack surface is thus

$$\boldsymbol{\sigma} = 10^{-3}\mu \begin{pmatrix} 0 & 0 & 2 \\ 0 & 0 & 0 \\ 2 & 0 & 4 \end{pmatrix}.$$

Selecting and appropriate value for the constant α, and using equation (8), for the Burgers vector of each crack dislocation, we obtain plane.

$$\mathbf{b} = \begin{pmatrix} -0.05 \\ 0 \\ -0.1 \end{pmatrix}.$$

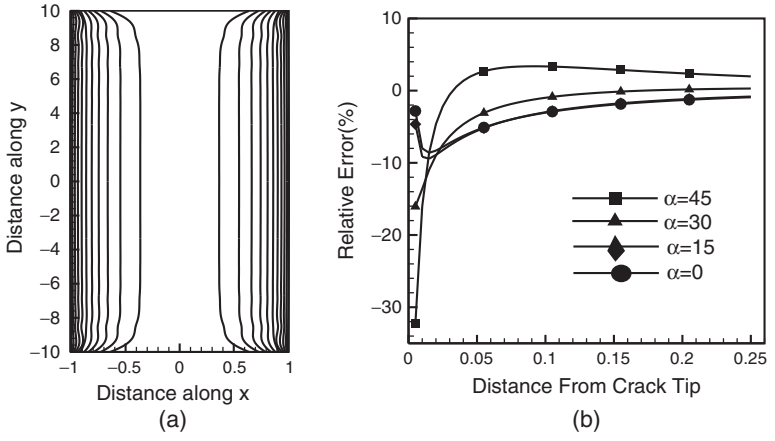

Figure 9. Griffith crack under mixed mode I & II loading. (a) Crack dislocation distribution. (b) The relative error of σ_{zx} along different angles α from the x-axis.

The equilibrium distribution of crack dislocations is shown in figure 9a, where we used a total of 22 crack dislocations. Unlike the previous case of a Griffith crack in pure mode-I or mode-II loading, all representative dislocations here have a mixed character of their Burgers vector. We show the dependence of the relative percent error in σ_{xx} on the distance ahead of the crack tip at different angles α from the x-axis in figure 9b. As shown in the figure, when the distance is larger than $10a$, the relative error decreases to less than 5% for a 22-dislocation representation of the crack. Shallower orientations from the x-axis (i.e. smaller values of α) are found to have smaller relative errors, as can be seen in figure 9b.

4.2. *Branched grain boundary crack*

In poly-crystalline materials, inter-granular failure proceeds by a process of separation between adjacent grain boundary surfaces. The separation may be over a small area, or may extend throughout the entire grain boundary, thus totally separating two adjacent grains. In this case, a three-dimensional crack is formed with the external contour conforming to grain edges. For fracture to proceed further, separated grain boundary surfaces will have to branch onto neighbouring grains, and a case of a branched grain boundary crack is formed. We will treat both possibilities here.

Grain boundaries may be hexagonal, although other polygonal shapes are observed. For illustrative purposes with no loss of generality, however, we present here the stress field characteristics of a fully de-bonded hexagonal boundary under an external tensile load of $\sigma_{zz}/\mu = 0.0033$. Figure 10a shows the equilibrium position of representative crack dislocation loops, where we fixed the outer hexagonal loop and used the techniques described earlier to determine the distribution, number, and configuration of inserted loops. Only 12 concentric loops were found to sufficiently represent the grain boundary crack. The 3-dimensional shape of the crack is shown in figure 10b, while the σ_{zz} iso-surfaces are shown in figures 10c and 10d, for a stress value 10 and 6 times the applied stress, respectively.

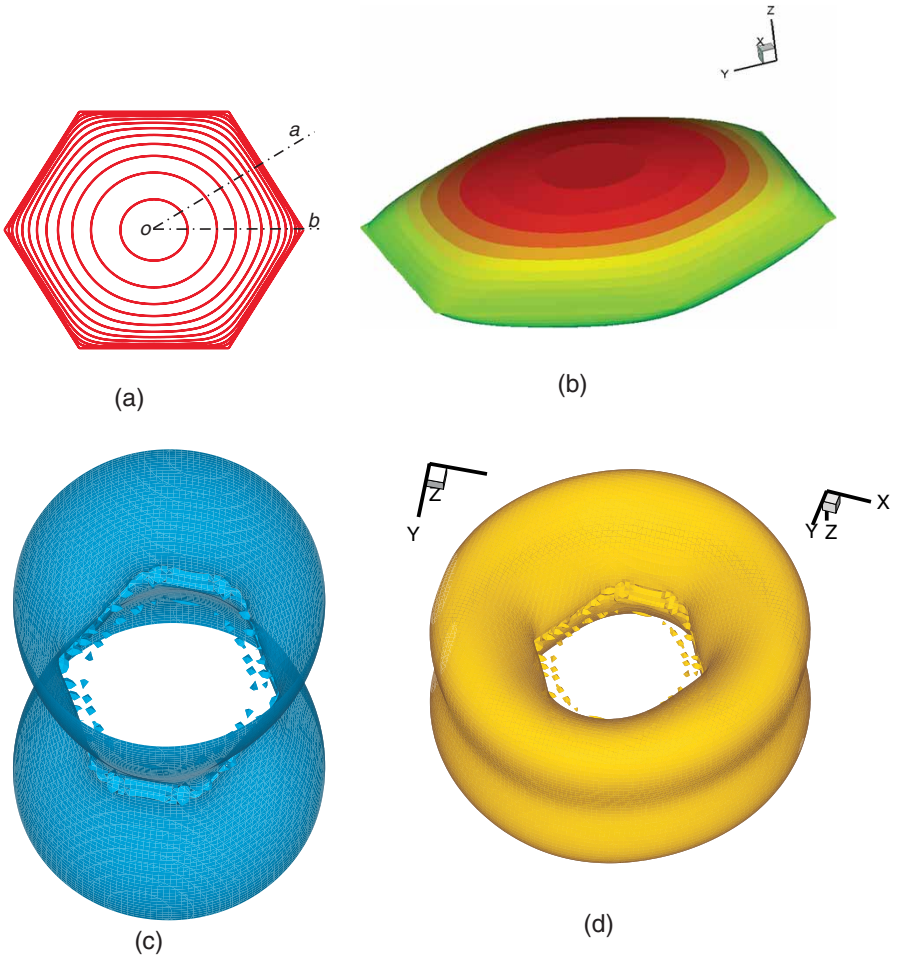

Figure 10. Characteristics of a grain boundary crack on a hexagonal face, (a) Discrete loop representation, (b) 3-D shape of crack opening, (c) stress iso-surface $\sigma_{zz}/\sigma_a = 10$, (d) stress iso-surface $\sigma_{zz}/\sigma_a = 6$.

Let us now assume that a grain boundary crack, with a hexagonal bounding contour, has now branched in between neighbouring grain boundaries. We take a case of symmetric branching on two inclined planes at 60° from the horizontal $z = 0$ plane. We represent this crack with a set of non-coplanar crack dislocation loops, with the outer loop fixed at the specified branched crack boundary. The equilibrium configuration of the concentric loop set is shown in figure 11. The resulting 3-dimensional crack shape under the same applied loading of $\sigma_{zz}/\mu = 0.0033$ is shown in figure 12. The set of figures 13 are representative of the stress field σ_{zz} on various planes, where 13a–13c are on the planes $x = 0$, $x = 866$, and $x = 1000$, respectively. At $x = 0$, we see two singularities, at $x = 866$ they collapse into only one (the hexagon apex), and at $x = 1000$, the field is regular because it is outside the crack surface. Similar observations can be obtained from figures 13d–13f. Contours on the z-planes are all outside the crack, and are thus

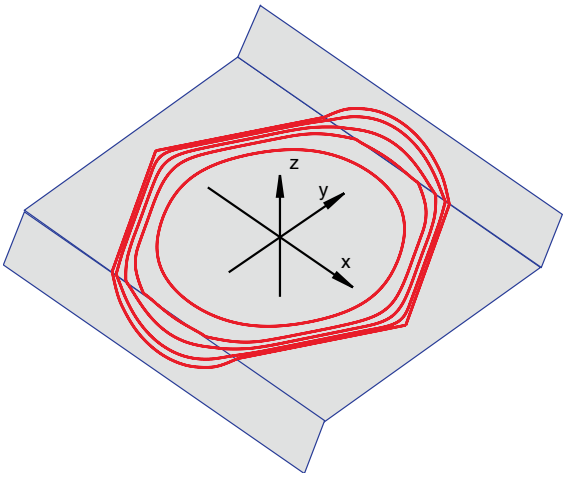

Figure 11. Crack dislocation loop distribution and coordinates under an external loading of $\sigma_{zz}/\mu = 0.0033$ for the branched grain boundary crack.

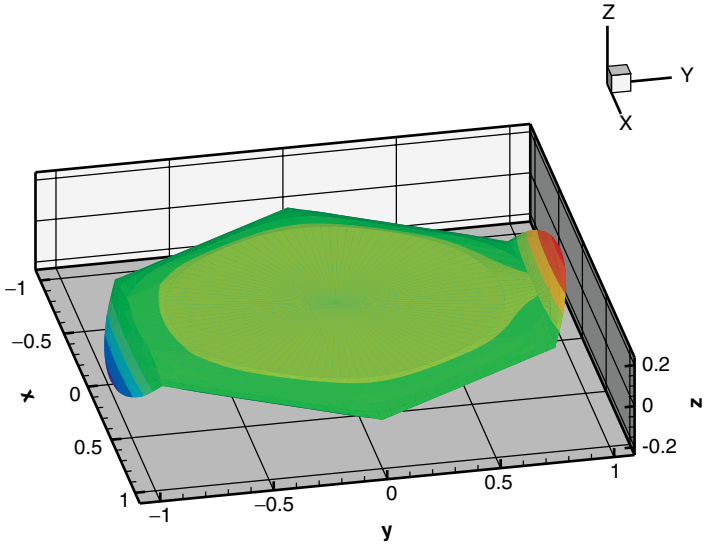

Figure 12. COD profile for the branched grain boundary crack. Note that the displacement is enlarged 25 times to allow visualization.

regular. Figure 14 shows a two-dimensional plot for the Crack Opening displacement (COD), and thus the crack profile on the $x = 0$ plane. Note that the crack surface is almost flat in the central zone.

5. Conclusions

Based on the method of Parametric Dislocation Dynamics (PDD), a new approach has been developed for determination of the stress field of 3-dimensional cracks of

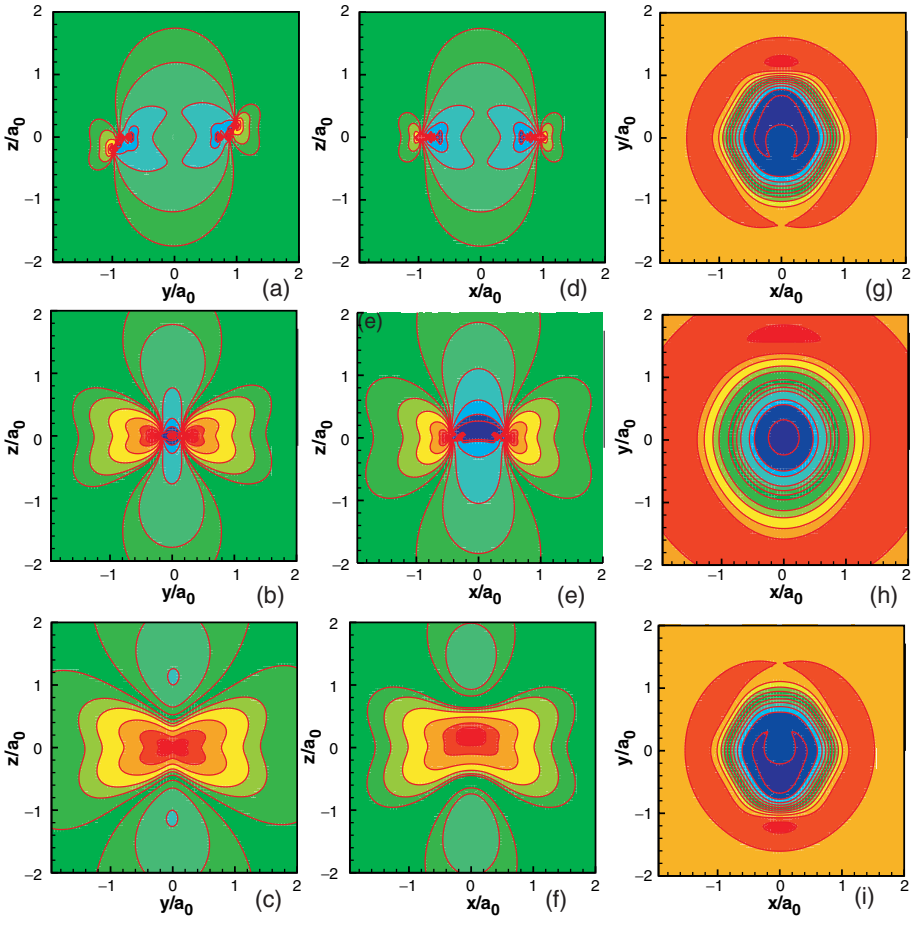

Figure 13. Stress contours for the branched grain boundary crack. Contours are for stresses on the following planes: (a) $x=0$, (b) $x=866$, (c) $x=1000$, (d) $y=0$, (e) $y=866$, (f) $y=1121$, (g) $z=500$, (h) $z=1000$, (i) $z=-500$.

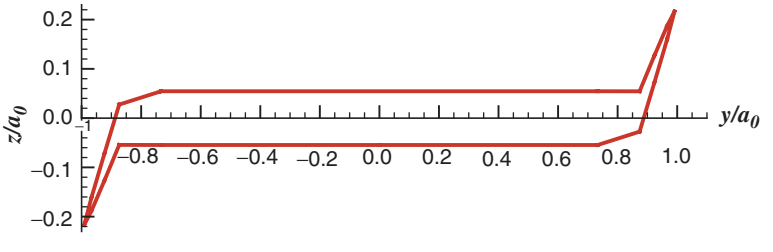

Figure 14. Crack Opening Displacement (COD) of the crack at the $x=0$ plane.

general and complex shapes. The main idea is that we parameterize the external shape of the crack by sets of Somigliana crack dislocation loops, where the Burgers vector is a local property determined from the local stress tensor and the normal vector to the crack surface at the point of interest. The distribution and number of

crack dislocation loops is determined by satisfying the equilibrium and stability conditions for the set of representative loops. The method has been demonstrated to be very accurate, with controlled and convergent precision for some well-known cases of 3D cracks, namely the penny-shape and the Griffith cracks. Error control is dependent on where the solution is desired, with more stringent requirements close to the crack tip. Higher accuracy follows from the numerical studies of the PDD [17], where the number of integration quadrature points and their distribution has a direct bearing on the desired error.

Due to its relative simplicity compared to other methods for 3-D cracks that rely on hyper singular integral solution techniques, the present approach offers some definite computational advantages. Moreover, since the approach is an extension of the well-established PDD for dislocation dynamics, much of the same techniques can be used for large-scale computations involving multiple complex-shape cracks, as well as crack-dislocation ensembles.

References

[1] J.D. Eshelby, F.C. Frank and F.R.N. Nabarro, The equilibrium of linear arrays of dislocations, Phil. Mag. **42** 351 (1951).
[2] J. Friedel, *Fracture*, chapter 24 (Wiley, New York, 1959), pp. 498–523.
[3] B.A. Bibly and J.D. Eshelby, *Fracture* (Wiley, New York, 1968).
[4] R.W. Lardner, *Mathematical Theory of Dislocations and Fracture* (University of Toronto Press, 1974).
[5] Johannes Weertman, *Dislocation Based Fracture Mechanics* (World Scientific Publishing Co. Pte. Ltd., 1996).
[6] B.A. Bilby, A.H. Cottrell and K.H. Swinden, The spread of plastic yield from a notch, Proc. Roy. Soc. Ser A **272** 304 (1963).
[7] G. Leibfried, Z. Phys. **130** 214 (1951).
[8] J. Friedel *Les Dislocations* (Gauthier-Villars, Paris, 1956).
[9] J.M. Burgers, Some considerations on the field of stress connected with dislocations in a regular crystal lattice, Proc. K. Ned. Akad. **42** 293 (1939).
[10] F.R.N. Nabarro, The synthesis of elastic dislocation fields, Phil. Mag. **42** 1224 (1951).
[11] D.A. Hills, P.A. Kelly, D.N. Dai and A.M. Korsunsky, *Solution of Crack Problems, the Distributed Dislocation Technique* (Kluwer Academic Publisher, 1996).
[12] N.M. Ghoniem and L.Z. Sun, Fast sum method for the elastic field of 3-D dislocation ensembles, Phy Rev B **60** 128 (1999).
[13] N.M. Ghoniem, Curved parametric segments for the stress field of 3-D dislocation loops, Transactions of ASME. J. Eng. Mat. & Tech. **121** 136 (1999).
[14] N.M. Ghoniem, S.-H. Tong and L.Z. Sun, Parametric dislocation dynamics: A thermodynamics-based approach to investigations of mesoscopic plastic deformation, Phys. Rev. **61** 913 (2000).
[15] N.M. Ghoniem, J. Huang and Z. Wang, Affine covariant-contravariant vector forms for the elastic field of parametric dislocations in isotropic crystals, Phil. Mag. Lett. **82** 55 (2001).
[16] H.F. Bueckner, The propagation of cracks and the energy of elastic deformation, J. Appl. Mech. **35** 1225 (1958).
[17] Jianming Huang and Nasr M. Ghoniem, Accuracy and convergence of parametric dislocation dynamics, Modelling Simul. Mater. Sci. Eng. **11** 21 (2003).

[18] N.M. Ghoniem and L.Z. Sun, Fast sum method for the elastic field of 3-d dislocation ensembles, Phys. Rev. B **60** (1999).
[19] R. Sack, Proc. Phys. Soc. **58** 729 (1946).
[20] I.N. Sneddon, The distribution of stress in the neighbourhood of a crack in an elastic solid, Proc. Roy. Soc. **187** 229 (1946).
[21] W.D. Collins, Some axially symmetric stress distributions in elastic solids containning penny-shaped cracks. i. cracks in an infinite solid and a thick plate, Proc. Roy. Soc. **266** 359 (1962).
[22] M.K. Kassir and G.C. Sih, Three-dimensional stress distribution around an elliptical crack under arbitrary loading, Journal of Applied Mechanics, Trans. ASME **33** 601 (1966).
[23] Zhiqiang Wang, Nasr M. Ghoniem and Richard LeSar, Multipole representation of the elastic field of dislocation ensembles. *Phys. Rev. B*, **69** 174102-1 to 174102-7 (2004).